

An Instance Segmentation Dataset of Yeast Cells in Microstructures

Christoph Reich^{1,*}, Tim Prangemeier^{1,*}, André O. Françani², Heinz Koepl^{1,‡}

Abstract—Extracting single-cell information from microscopy data requires accurate instance-wise segmentations. Obtaining pixel-wise segmentations from microscopy imagery remains a challenging task, especially with the added complexity of microstructured environments. This paper presents a novel dataset for segmenting yeast cells in microstructures. We offer pixel-wise instance segmentation labels for both cells and trap microstructures. In total, we release 493 densely annotated microscopy images. To facilitate a unified comparison between novel segmentation algorithms, we propose a standardized evaluation strategy for our dataset. The aim of the dataset and evaluation strategy is to facilitate the development of new cell segmentation approaches. The dataset is publicly available at https://christophreich1996.github.io/yeast_in_microstructures_dataset/.

I. INTRODUCTION

Many biomedical applications require the detection and segmentation of individual cells in microscopy imagery [1]. For example, analyzing the cellular processes of living cells in time-lapse fluorescence microscopy (TFLM) experiments, requires accurate pixel-level segmentations of individual cells [2]–[5]. Most applications require each cell to be segmented and identified as a unique entity or instance [6]. Instance segmentation is the task of detecting, segmenting, and classifying each object instance in an image [7]. While powerful cell segmentation algorithms have been proposed recently (*e.g.* [8], [9]), segmenting cells in microstructured environments remains challenging, due to the perceptual similarity of microstructures and cells (*cf.* Fig. 1) [3], [10], [11].

The vast majority of current state-of-the-art segmentation algorithms utilize deep neural networks [9], [12]–[14]. A key factor driving the development of deep learning-based segmentation algorithms is the widespread availability of pixel-wise annotated datasets. Examples include Microsoft COCO [15], Cityscapes [7], ADE20K [16], and the 2018 Data Science Bowl dataset [17]. While general cell segmentation datasets are available (*e.g.* [17], [18]), we are not aware of any instance segmentation dataset of cells in microstructures with dense annotations.

In this paper, we present and publicly release a dataset of yeast (*Saccharomyces cerevisiae*) cells in microstructures with instance segmentation annotations. The dataset is comprised of 493 densely annotated brightfield microscopy images of different TFLM experiments (*cf.* Fig. 1). To facilitate a fair comparison between novel

segmentation approaches we also propose a standardized performance evaluation strategy. The PyTorch [19] code for performance evaluation is publicly available at <https://github.com/ChristophReich1996/Yeast-in-Microstructures-Dataset>.

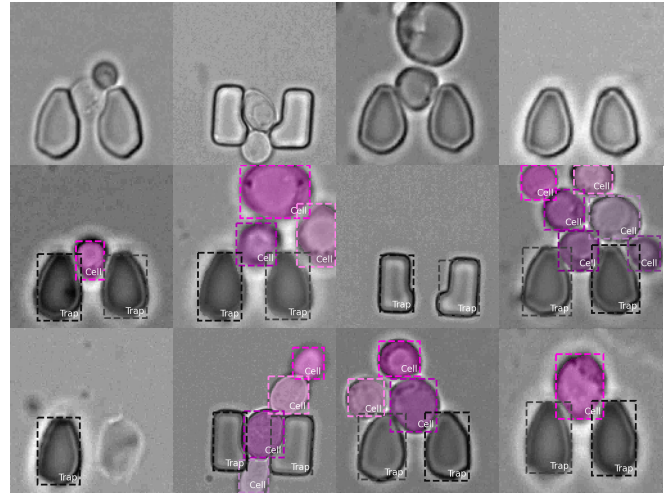


Fig. 1. Samples of our yeast cells in microstructures dataset. The top row show unlabelled brightfield imagery to demonstrate the visual similarity between the cells and similarly sized microstructures. In the following rows, the instance segmentation labels are overlaid onto the the brightfield microscopy imagery (grayscale). A bounding box and object class label denotes each object for clarity. Shades of pink (■) indicate individual cell instances and shades of (dark) gray (■) indicate microstructures (traps).

II. DATASET

When developing a segmentation dataset, numerous design choices have to be made. This section will give a detailed overview of these design decisions. First, we describe the data acquisition and annotation process. Second, we will introduce the core features and statistics of our dataset. Finally, we describe how our dataset is split for training, validation, and testing.

A. Data Acquisition

We chose two common yeast trap microstructure geometries and drew data from a wide range of experiments performed in our lab to generate our dataset (*cf.* Fig. 1) [20], [21]. An overview of the experimental setup atop the microscope table is given in Fig. 2. We designed and fabricated trap microchips for long-term cultures of yeast cells (*cf.* Fig. 2). We recorded brightfield microscopy images of the living yeast cells confined to the microfluidic chip over many hours. A constant flow of yeast growth media hydrodynamically traps the cells in the microstructure pairs [4], [22].

* Christoph Reich & Tim Prangemeier - both authors contributed equally

‡ Correspondence: heinz.koepl@tu-darmstadt.de

¹ Centre for Synthetic Biology, Department of Electrical Engineering and Information Technology, Technische Universität Darmstadt

² Aeronautics Institute of Technology, work done while at TU Darmstadt

We extracted 493 specimen images, each centered on a single trap microstructure pair with a resolution of 128×128 , from the higher resolution raw data, as is common practice (cf. Fig. 2) [3], [21]. We differentiate between two subsets, one for each of the trap geometries employed (roughly oval shaped *regular traps*, and the *L traps*). In order to increase the robustness and range of applicability of the models trained on this data, we include variations in trap type, debris, focal shift illumination levels, and yeast morphology. Our dataset captures the most common yeast-trap configurations: (i) empty traps (ii) single cells (with daughter) and (iii) multiple cells [6]. Our dataset also includes edge cases such as broken traps (cf. Fig. 1 bottom left).

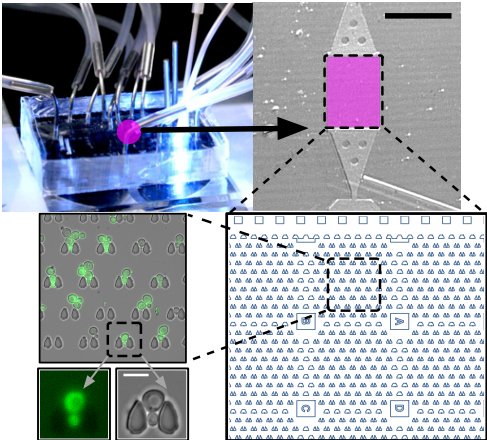


Fig. 2. TLFM experiment setup for single-cell fluorescence measurement. A microfluidic chip sits atop the microscope table (top left). The trap chamber (pink \blacksquare on the top right) contains approximately one thousand traps. We extract cropped specimen images from the fluorescence and brightfield channels (bottom left), that include a pair of trap microstructures and cells. The brightfield channel is used for segmentation (and in this dataset). The black scale bar is 1mm, the white scale bar is $10\mu\text{m}$.

B. Data Annotation

We present 493 pixel-level annotated images, with pixel-wise instance-level annotations of both cells and microstructures (traps). Each pixel, not labeled as a cell or trap, is considered as background. Note, since our labels only include a single background class, our instance segmentation labels can also be seen as panoptic labels [23]. This property is later used for performance evaluation (cf. Section III).

All annotations were acquired manually. For every object instance (cells and traps), we annotate the object class and the pixels belonging to the object. Note that we assume no overlapping cell and trap instances (seeing as the chips are designed to prevent any overlap). This annotation process results in a binary segmentation map and classification for each object instance. Fig. 3 showcases both brightfield images and our manual instance-wise annotations.

In most cases, cell instances can easily be distinguished during labeling. In the case of budding, in which a daughter cell pinches off a mother cell, labeling the growing daughter cell is non-trivial [24]. We decided to annotate the daughter cell as a separate instance if it is clearly separated from the mother cell. An example of this is given in Fig. 3 (bottom

right). The detection of daughter cells, can, for example, aid in determining the cell fitness.

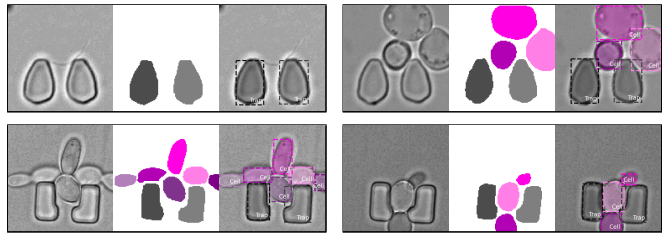


Fig. 3. Brightfield microscopy imagery of yeast cells and microstructures with the corresponding labels. Brightfield images on the left, instance segmentation label in the middle, and an overlay of the brightfield images and labels on the right. Shades of gray (\blacksquare) indicate different instances of microstructures (trap). Cell instances are visualized in shades of pink (\blacksquare). The background is white.

While most applications, such as analyzing the cellular process of living cells, mainly require the segmentation of cells, we decided to also include annotations of microstructures in our dataset. The reason for this decision is twofold. First, when knowing both the position cells and traps it can be determined which cells are hydrodynamically trapped and which cells are outside of the trap, likely to be hydrodynamically washed out of the chip. Second, learning the difference between cells and traps might be enforced by explicitly learning to also segment each trap instance.

C. Dataset Statistics

Our full dataset is comprised of two distinct subsets, one for each of the trap geometries (*regular* and *L traps*). Details on the core features of both subsets are depicted in Table I. The first subset includes *regular* trap types, and slight variations of this geometry, also referred to as type 1, whereas the second subset includes *L-shaped* traps (type 2). In general, the first subset includes approximately four times the number of images and object instances (cells and traps) as the second subset.

TABLE I
CORE PROPERTIES OF OUR CELLS IN MICROSTRUCTURES DATASET.

	Trap type	# images	# cells	# traps
Subset 1	Type 1 (<i>regular</i>)	398	702	781
Subset 2	Type 2 (<i>L</i>)	95	212	190
Full dataset	Type 1 & 2	493	914	971

We analyze the number of instances per class in each specimen image. Fig. 4 shows the histogram of instances per image for both subsets and both semantic classes. The majority of images include two traps and at least a single cell. However, our dataset also includes specific edge cases, such as the case where only a single intact trap microstructure instance is present due to fabrication errors. In the most common setting, two cells and two trap instances are present. This corresponds to the setting of a trapped mother cell with a budding daughter cell that pinches off from the mother cell [24]. Images without any cells are also included. The maximum number of cells in a single image is six.

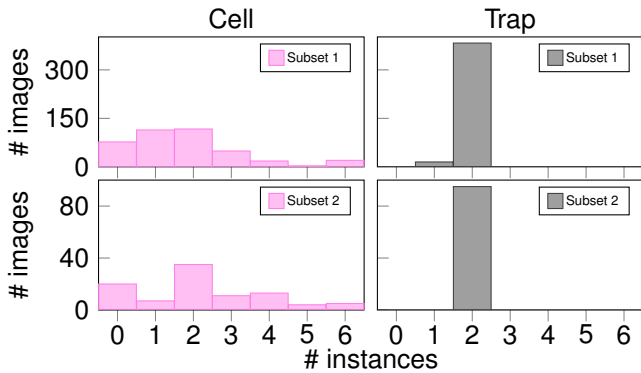


Fig. 4. Histogram showing the frequency of number of object instances in an image of our dataset. Left column visualizes the cell class (pink \blacksquare) and right column the trap class (grey \blacksquare).

Our dataset includes yeast cells of vastly different sizes. This is showcased in Fig. 5, where the cell size distribution approximately follows a normal distribution. The first subset, however, includes some outliers in the form of very large cells. The trap size histogram (*cf.* Fig. 5) exhibits less variance than that of the cells (as is expected for microfabricated structures). The variation in trap appearance is included for increased model robustness and is due to a range of factors, ranging from fabrication tolerances, the position of the focal plane, to mechanical chip deformations (bending, warping, inclined mounting), amongst others.

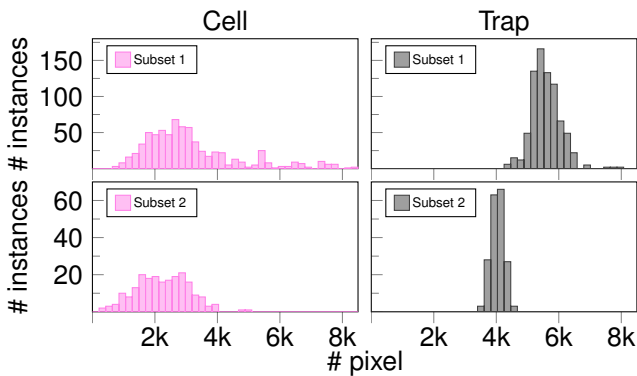


Fig. 5. Histogram of object instance sizes in number of pixels. Left column visualizes the class cell (pink \blacksquare) and right column the class trap (grey \blacksquare).

The distribution of cell positions is depicted as a density map in Fig. 6. Yeast cells are mainly located inside a trap pair (*cf.* Fig. 6). Additional cells are typically located above the trap pair. When budding, the daughter cell typically grows near the top of the microstructures. In some cases, daughter cells grow out of the bottom of the trap.

D. Dataset Splits

Our densely annotated microscopy images are split into three separate sets for training, validation, and testing. We initially split the dataset randomly. However, we subsequently manually curated the sets to ensure that all splits include a similar amount of variability in cell and trap configurations. Following the split fraction of the Cityscapes

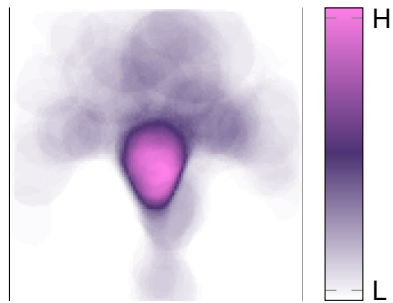


Fig. 6. Density map of cell locations in our dataset. Pink (\blacksquare) areas indicate regions where many cells are located (H). White areas showcase regions where only a few or even no cells are located (L).

dataset ($\sim 60\%$ training, $\sim 10\%$ validation, and $\sim 30\%$ test), we arrive at a split consisting of 296 training, 49 validation, 148 test images with dense annotations. Table II presents details of the dataset split.

TABLE II
TRAINING, VALIDATION, AND TEST SPLIT OF OUR DATASET.

Split	# images	# cells	# traps	Trap type images 1 vs. 2
Training	296	536	582	244/52
Validation	49	108	98	33/16
Test	148	270	291	121/27

III. PERFORMANCE EVALUATION

We propose to utilize both the cell class intersection-over-union (IoU) and the panoptic quality (PQ) metrics [23] to evaluate instance segmentation algorithms on our dataset. The cell class IoU (Jaccard index) is defined as:

$$\text{IoU}(p_c, g_c) = \frac{|p_c \cap g_c|}{|p_c \cup g_c|}, \quad (1)$$

where p_c is the segment for the cell class and g_c indicates the cell class ground truth. This metric evaluates the semantic performance of the cell segmentation. While we are presenting an instance segmentation dataset, we propose to validate the performance of instance segmentation approaches on our dataset with the cell class IoU to ensure a comparison between previous work which utilizes this metric [3], [6], [11], [25]. The cell class IoU is biased towards large objects and does not capture the recognition and segmentation of individual object instances. However, when an application does not require single-cell segmentations but the semantic segmentation of all cells, this metric is an insightful measure of the semantic segmentation performance.

To measure the instance segmentation performance on our yeast cells in microstructures dataset, we propose to utilize the PQ metric. In panoptic segmentation, object classes are categorized into two different class types. First, “stuff classes” include uncountable objects/regions such as sidewalks or grass. Second, “things classes” include countable objects classes, such as cars, people, or bicycles. For stuff classes, semantic segmentation is performed, whereas instance segmentation is performed for things classes. Our

instance segmentation dataset can be seen as an edge-case of panoptic segmentation. Cell and trap classes can be viewed as things classes, whereas the background builds the only stuff class. Thus, we can evaluate an instance segmentation prediction for our dataset with the PQ.

The PQ is computed individually for each semantic class (background, cell, & trap) and averaged over all classes. Before computing the PQ for a class, the predicted and labeled instances are matched. This matching results in three sets: true positive (TP), false positive (FP), and false negative (FN) matches. Please refer to Kirillov *et al.* [23] for details on the matching approach. Based on these sets the PQ is computed for each semantic class as:

$$PQ = \underbrace{\frac{\sum_{(p,g) \in TP} \text{IoU}(p,g)}{|\text{TP}|}}_{SQ} \underbrace{\frac{|\text{TP}|}{|\text{TP}| + \frac{1}{2}|\text{FP}| + \frac{1}{2}|\text{FN}|}}_{RQ}, \quad (2)$$

here $\frac{1}{|\text{TP}|} \sum_{(p,g) \in TP} \text{IoU}(p,g)$ computes the mean IoU of all matched predicted p and ground truth g segments. The PQ is a measure of both the (instance-wise) segmentation quality (SQ) and the recognition quality (RQ) of a panoptic segmentation prediction. Additionally, the PQ weights each object instance importance independent of their size.

By measuring both the cell class IoU and the PQ, we can evaluate the performance of segmentation algorithms on our instance segmentation dataset. For applications requiring single-cell segmentations and the positioning and segmentation of microstructures, the PQ is the superior metric. The cell class IoU is to be preferred for applications requiring only semantic information of cells. We offer code for computing both the cell class IoU and the panoptic quality for a standardized comparison of new approaches.

IV. CONCLUSION AND OUTLOOK

In this paper, we presented a new dataset for segmenting yeast cells in microstructures, a widespread scenario for a key model organism in biological research and development. We provide both pixel-wise instance segmentation labels and a standardized performance evaluation strategy. The aim of this joint approach is to facilitate progress in the field of trapped yeast analysis and to provide a basis for a fair comparison between instance segmentation methods.

Beyond the scenario presented here, some biomedical applications require temporal cell segmentations. To aid the development of unified cell segmentation and tracking algorithms, future work may consider extending our dataset with video instance segmentation labels [26].

ACKNOWLEDGMENT

We thank Christoph Hoog Antink for insightful discussions, Klaus-Dieter Voss for aid with the microfluidics fabrication, and Jan Basrawi for contributing to data labelling.

This work was supported by the Landesoffensive für wissenschaftliche Exzellenz as part of the LOEWE Schwerpunkt CompuGene. H.K. acknowledges the support from the European Research Council (ERC) with the consolidator

grant CONSYN (nr. 773196). C.R. acknowledges the support of NEC Laboratories America, Inc.

REFERENCES

- [1] E. Meijering, "Cell Segmentation: 50 Years Down the Road," *IEEE Signal Process. Mag.*, vol. 29, no. 5, pp. 140–145, 2012.
- [2] R. Pepperkok and J. Ellenberg, "High-throughput fluorescence microscopy for systems biology," *Nat. Rev. Mol. Cell Biol.*, vol. 7, no. 9, pp. 690–696, 2006.
- [3] E. Bakker, P. S. Swain, and M. M. Crane, "Morphologically constrained and data informed cell segmentation of budding yeast," *Bioinformatics*, vol. 34, no. 1, pp. 88–96, 2018.
- [4] T. Prangemeier, F.-X. Lehr, R. M. Schoeman, and H. Koepl, "Microfluidic platforms for the dynamic characterisation of synthetic circuitry," *Curr. Opin. Biotechnol.*, vol. 63, pp. 167–176, 2020.
- [5] T. Aspert, D. Hentsch, and G. Charvin, "DetecDiv, a generalist deep-learning platform for automated cell division tracking and survival analysis," *eLife*, vol. 11, p. e79519, 2022.
- [6] T. Prangemeier, C. Reich, and H. Koepl, "Attention-Based Transformers for Instance Segmentation of Cells in Microstructures," in *IEEE BIBM*, 2020, pp. 700–707.
- [7] M. Cordts, M. Omran, S. Ramos, T. Rehfeld, M. Enzweiler, R. Benenson, U. Franke *et al.*, "The Cityscapes Dataset for Semantic Urban Scene Understanding," in *CVPR*, 2016, pp. 3213–3223.
- [8] U. Schmidt, M. Weigert, C. Broaddus, and G. Myers, "Cell Detection with Star-Convex Polygons," in *MICCAI*, 2018, pp. 265–273.
- [9] C. Stringer, T. Wang, M. Michaelos, and M. Pachitariu, "Cellpose: a generalist algorithm for cellular segmentation," *Nat. Methods*, vol. 18, no. 1, pp. 100–106, 2021.
- [10] A. O. Françani, "Analysis of the performance of U-Net neural networks for the segmentation of living cells," *arXiv:2210.01538*, 2022.
- [11] T. Prangemeier, C. Wildner, A. O. Françani, C. Reich, and H. Koepl, "Yeast cell segmentation in microstructured environments with deep learning," *Biosystems*, vol. 211, p. 104557, 2022.
- [12] K. He, G. Gkioxari, P. Dollár, and R. Girshick, "Mask R-CNN," in *CVPR*, 2017, pp. 2961–2969.
- [13] C. H. Antink, J. C. M. Ferreira, M. Paul, S. Lyra, K. Heimann, S. Karthik, J. Joseph, K. Jayaraman, T. Orlikowski *et al.*, "Fast body part segmentation and tracking of neonatal video data using deep learning," *Med. Biol. Eng. Comput.*, vol. 58, pp. 3049–3061, 2020.
- [14] C. Reich, T. Prangemeier, Ö. Cetin, and H. Koepl, "OSS-Net: Memory Efficient High Resolution Semantic Segmentation of 3D Medical Data," in *BMVC*, 2021.
- [15] T.-Y. Lin, M. Maire, S. Belongie, J. Hays, P. Perona, D. Ramanan, P. Dollár, and C. L. Zitnick, "Microsoft COCO: Common Objects in Context," in *ECCV*, 2014, pp. 740–755.
- [16] B. Zhou, H. Zhao, X. Puig, S. Fidler *et al.*, "Scene Parsing Through ADE20K Dataset," in *CVPR*, 2017, pp. 633–641.
- [17] J. C. Caicedo, A. Goodman, K. W. Karhohs, B. A. Cimini *et al.*, "Nucleus segmentation across imaging experiments: the 2018 Data Science Bowl," *Nat. Methods*, vol. 16, no. 12, pp. 1247–1253, 2019.
- [18] S. Parekh and S. Mischa, "EVICAN Dataset," 2019.
- [19] A. Paszke, S. Gross, F. Massa, A. Lerer, J. Bradbury, G. Chanan, T. Killeen, Z. Lin *et al.*, "PyTorch: An Imperative Style, High-Performance Deep Learning Library," in *NeurIPS*, vol. 32, 2019.
- [20] M. M. Crane, I. B. Clark, E. Bakker *et al.*, "A Microfluidic System for Studying Ageing and Dynamic Single-Cell Responses in Budding Yeast," *PLOS ONE*, vol. 9, no. 6, pp. 1–10, 2014.
- [21] C. Reich, T. Prangemeier, C. Wildner, and H. Koepl, "Multi-StyleGAN: Towards Image-Based Simulation of Time-Lapse Live-Cell Microscopy," in *MICCAI*, 2021.
- [22] T. Prangemeier, C. Wildner, M. Hanst, and H. Koepl, "Maximizing Information Gain for the Characterization of Biomolecular Circuits," in *ACM NanoCom*, 2018, pp. 1–6.
- [23] A. Kirillov, K. He, R. Girshick, C. Rother, and P. Dollár, "Panoptic Segmentation," in *CVPR*, 2019, pp. 9404–9413.
- [24] A. A. Duina, M. E. Miller, and J. B. Keeney, "Budding Yeast for Budding Geneticists: A Primer on the *Saccharomyces cerevisiae* Model System," *Genetics*, vol. 197, no. 1, pp. 33–48, 2014.
- [25] T. Prangemeier, C. Wildner, A. O. Françani, C. Reich, and H. Koepl, "Multiclass Yeast Segmentation in Microstructured Environments with Deep Learning," in *IEEE CIBCB*, 2020, pp. 1–8.
- [26] L. Yang, Y. Fan, and N. Xu, "Video instance segmentation," in *ICCV*, 2019, pp. 5188–5197.